Universiteit Gent
Faculteit Wetenschappen
Vakgroep Fysica en Sterrenkunde

No title yet
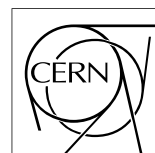
No sub-title neither, obviously...

Alexis Fagot

Thesis to obtain the degree of
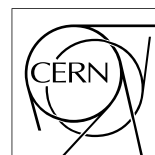Doctor of Philosophy in Physics
Academic years 2012-2017

Acknowledgements

Ici on remerciera tous les gens que j'ai pu croiser durant cette aventure et qui m'ont permis de passer un bon moment

Gent, ici la super date de la mort qui tue de la fin d'écriture
Alexis Fagot

Table of Contents

List of Figures

List of Tables

List of Acronyms

List of Acronyms

A

AFL   Almost Full Level

B

BARC   Bhabha Atomic Research Centre
BLT   Block Transfer
BR   Branching Ratio

C

CAEN   Costruzioni Apparecchiature Elettroniche Nucleari S.p.A.

CERN   European Organization for Nuclear Research
CFD   Constant Fraction Discriminator
CMS   Compact Muon Solenoid
CSC   Cathode Strip Chamber

D

DAQ   Data Acquisition
DCS   Detector Control Software
DQM   Data Quality Monitoring

DT	Drift Tube

F

FEE	Front-End Electronics
FEB	Front-End Board

G

GE-/-	Find a good description
GE1/1	Find a good description
GE2/1	Find a good description
GEANT	GEometry ANd Tracking - a series of software toolkit platforms developed by CERN
GEM	Gas Electron Multiplier
GIF	Gamma Irradiation Facility
GIF++	new Gamma Irradiation Facility

H

HL-LHC	High Luminosity LHC
HV	High Voltage

I

iRPC	improved RPC
IRQ	Interrupt Request

L

LHC	Large Hadron Collider
LS1	First Long Shutdown
LS3	Third Long Shutdown

307	LV	Low Voltage
308	LVDS	Low-Voltage Differential Signaling

M

313	MC	Monte Carlo
314	MCNP	Monte Carlo N-Particle
315	ME-/-	Find good description
316	ME0	Find good description

N

321	NIM	Nuclear Instrumentation Module logic signals

P

326	PMT	PhotoMultiplier Tube

R

331	RE-/-	Find a good description
332	RE2/2	Find a good description
333	RE3/1	Find a good description
334	RE3/2	Find a good description
335	RE4/1	Find a good description
336	RE4/2	Find a good description
337	RE4/3	Find a good description
338	RMS	Root Mean Square
339	ROOT	a framework for data processing born at CERN
340	RPC	Resistive Plate Chamber

S

345	SPS	Super Proton Synchrotron

T

TDC   Time-to-Digital Converter

W

webDCS   Web Detector Control System

Nederlandse samenvatting
–Summary in Dutch–

Le resume en Neerlandais (j'aurais peut-etre de apprendre la langue juste pour ca...).

English summary

Le meme résume mais en Anglais (on commencera par la hein!).

1
Introduction

2
Investigating the TeV scale

2.1 The Standard Model of Particle Physics

2.2 The Large Hadron Collider and the Compact Muon Solenoid

2.3 Muon Phase-II Upgrade

After the more than two years lasting First Long Shutdown (LS1), the Large Hadron Collider (LHC) delivered its very first Run-II proton-proton collisions early 2015. LS1 gave the opportunity to the LHC and to the its experiments to undergo upgrades. The accelerator is now providing collisions at center-of-mass energy of $13\,\mathrm{TeV}$ and bunch crossing rate of $40\,\mathrm{MHz}$, with a peak luminosity exceeding its design value. During the first and upcoming second LHC Long Shutdown, the Compact Muon Solenoid (CMS) detector is also undergoing a number of upgrades to maintain a high system performance [1].

From the LHC Phase-2 or High Luminosity LHC (HL-LHC) period onwards, i.e. past the Third Long Shutdown (LS3), the performance degradation due to integrated radiation as well as the average number of inelastic collisions per bunch crossing, or pileup, will rise substantially and become a major challenge for the LHC experiments, like CMS that are forced to address an upgrade program for Phase-II [2]. Simulations of the expected distribution of absorbed dose in the CMS detector under HL-LHC conditions, show in figure 5.14 that detectors placed close

388 to the beamline will have to withstand high irradiation, the radiation dose being of
389 the order of a few tens of Gy.
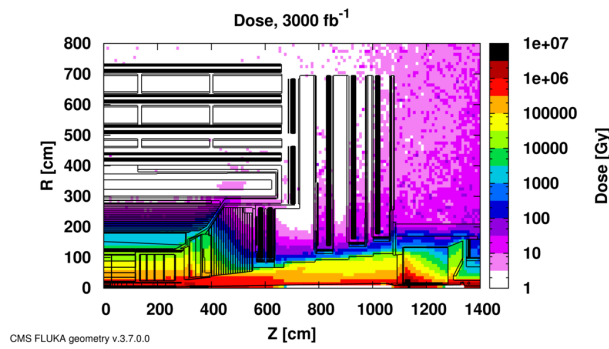
Figure 2.1: Absorbed dose in the CMS cavern after an integrated luminosity of 3000 fb. *R
is the transverse distance from the beamline and Z is the distance along the beamline from
the Interaction Point at Z=0.*

390   The measurement of small production cross-section and/or decay branching
391 ratio processes, such as the Higgs boson coupling to charge leptons or the $B_s \longrightarrow$
392 $\mu^+\mu^-$ decay, is of major interest and specific upgrades in the forward regions of
393 the detector will be required to maximize the physics acceptance on the largest
394 possible solid angle. To ensure proper trigger performance within the present cov-
395 erage, the muon system will be completed with new chambers. In figure 2.2 one
396 can see that the existing Cathode Strip Chambers (CSCs) will be completed by Gas
397 Electron Multipliers (GEMs) and Resistive Plate Chambers (RPCs) in the pseudo-
398 rapidity region $1.6 < |\eta| < 2.4$ to complete its redundancy as originally scheduled
399 in the CMS Technical Proposal [3].
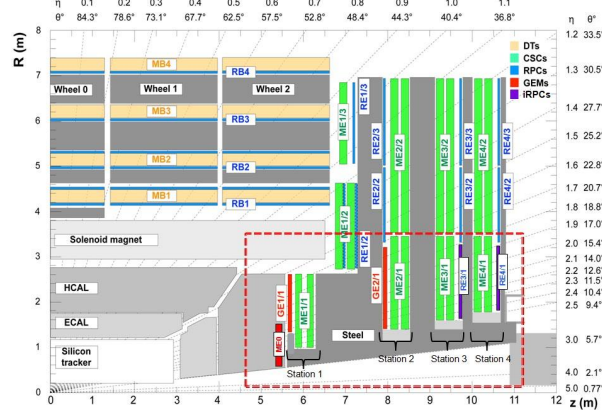
Figure 2.2: A quadrant of the muon system, showing DTs (yellow), RPCs (light blue), and CSCs (green). The locations of new forward muon detectors for Phase-II are contained within the dashed box and indicated in red for GEM stations (ME0, GE1/1, and GE2/1) and dark blue for improved RPC (iRPC) stations (RE3/1 and RE4/1).

RPCs are used by the CMS first level trigger for their good timing performances. Indeed, a very good bunch crossing identification can be obtained with the present CMS RPC system, given their fast response of the order of $1\,\text{ns}$. In order to contribute to the precision of muon momentum measurements, muon chambers should have a spatial resolution less or comparable to the contribution of multiple scattering [1]. Most of the plausible physics is covered only considering muons with $p_T < 100\,\text{GeV}$ thus, in order to match CMS requirements, a spatial resolution of $\mathcal{O}(\text{few mm})$ the proposed new RPC stations, as shown by the simulation in figure 2.3. According to preliminary designs, RE3/1 and RE4/1 readout pitch will be comprised between 3 and $6\,\text{mm}$ and 5 η-partitions could be considered.
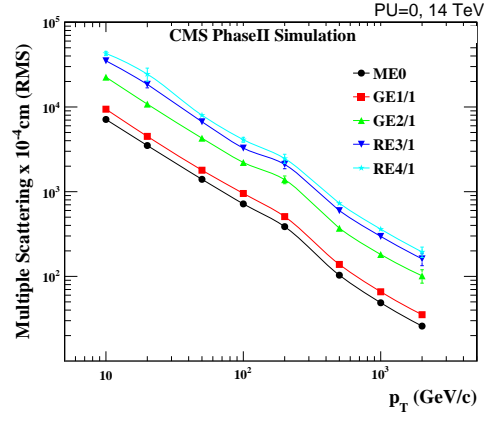
Figure 2.3:   RMS of the multiple scattering displacement as a function of muon p_T for the proposed forward muon stations. All of the electromagnetic processes such as bremsstrahlung and magnetic field effect are included in the simulation.

3

Amplification processes in gaseous detectors

3.1 Signal formation

3.2 Gas transport parameters

4

Resistive Plate Chambers

4.1 Principle

4.2 Rate capability of Resistive Plate Chambers

4.3 High time resolution

4.4 Resistive Plate Chambers at CMS

4.4.1 Overview

The Resistive Plate Chambers (RPC) system, located in both barrel and endcap regions, provides a fast, independent muon trigger with a looser p_T threshold over a large portion of the pseudorapidity range ($|\eta| < 1.6$) [add reconstruction].

During High-Luminosity LHC (HL-LHC) operations the expected conditions in terms of background and pile-up will make the identification and correct P_T assignment a challenge for the Muon system. The goal of RPC upgrade is to provide additional hits to the Muon system with precise timing. All these informations will be elaborated by the trigger system in a global way enhancing the performance of the trigger in terms of efficiency and rate control. The RPC Upgrade is based on two projects: an improved Link Board System and the extension of the RPC coverage up to $|\eta| = 2.4$. [FIXME 2.4 or 2.5?]

The Link Board system, that will be described in section xxx, is responsible to process, synchronize and zero-suppress the signals coming from the RPC front end boards. The Link Board components have been produced between 2006 and 2007 and will be subjected to aging and failure in the long term. The upgraded Link Board system will overcome the aging problems described in section xxx and will allow for a more precise timing information to the RPC hits from 25 to $1\,\mathrm{ns}$ [ref section xxx].

The extension of the RPC system up to $|\eta| = 2.1$ was already planned in the CMS TDR [ref cmstdr] and staged because of budget limitations and expected background rates higher than the rate capability of the present CMS RPCs in that region. An extensive R&D program has been done in order to develop an improved RPC that fulfills the CMS requirements. Two new RPC layers in the innermost ring of stations 3 and 4 will be added with benefits to the neutron-induced background reduction and efficiency improvement for both trigger and offline reconstruction.

4.4.2   The present RPC system

The RPC system is organized in 4 stations called RB1 to RB4 in the barrel region, and RE1 to RE4 in the endcap region. The innermost barrel stations, RB1 and RB2, are instrumented with 2 layers of RPCs facing the innermost (RB1in and RB2in) and outermost (RB1out and RB2out) sides of the DT chambers. Every chamber is then divided from the read-out point of view into 2 or 3 η partitions called "rolls". The RPC system consist of 480 barrel chambers and 576 endcap chambers. Details on the geometry are discussed in the paper [ref to geo paper].

The CMS RPC chamber is a double-gap, operated in avalanche mode to ensure reliable operation at high rates. Each RPC gap consists of two 2-mm-thick resistive High-Pressure Laminate (HPL) plates separated by a 2-mm-thick gas gap. The outer surface of the HPL plates is coated with a thin conductive graphite layer, and a voltage is applied. The RPCs are operated with a 3-component, non-flammable gas mixture consisting of 95.2% freon ($C_2H_2F_4$, known as R134a), 4.5% isobutane (i-C_4H_{10}), and 0.3% sulphur hexafluoride (SF_6) with a relative humidity of 40% - 50%. Readout strips are aligned in η between the 2 gas gaps. [Add a sentence on FEBs.]

The discriminated signals coming from the Front End boards feed via twisted cables (10 to $20\,\mathrm{m}$ long) the Link Board System located in UXC on the balconies around the detector. The Link System consist of the 1376 Link Boards (LBs) and the 216 Control Boards (CBs), placed in 108 Link Boxes. The Link Box is a custom crate (6U high) with 20 slots (for two CBs and eighteen LBs). The Link Box contains custom backplane to which the cables from the chambers are connected, as well as the cables providing the LBs and CBs power supply and the cables for the RPC FEBs control with use of the I2C protocol (trough the CB). The

backplane itself contains only connectors (and no any other electronic devices).

The Link Board has 96 input channels (one channel corresponds to one RPC strip). The input signals are the $\sim 100\,\text{ns}$ binary pulses which are synchronous to the RPC hits, but not to the LHC clock (which drives the entire CMS electronics). Thus the first step of the FEB signals processing is synchronization, i.e. assignment of the signals to the BXes (25 ns periods). Then the data are compressed with a simple zero-suppressing algorithm (the input channels are grouped into 8 bit partitions, only the partitions with at least one nonzero bit are selected for each BX). Next, the non-empty partitions are time-multiplexed i.e. if there are more than one such partition in a given BX, they are sent one-by-one in consecutive BXes. The data from 3 neighbouring LBs are concentrated by the middle LB which contains the optical transmitter for sending them to the USC over a fiber at $1.6\,\text{Gbps}$.

The Control Boards provide the communication of the control software with the LBs via the FEC/CCU system. The CBs are connected into token rings, each ring consists of 12 CBs of one detector tower and a FEC mezzanine board placed on the CCS board located in the VME crate in the USC. In total, there are 18 rings in the entire Link System. The CBs also perform automatic reloading of the LB's firmware which is needed in order to avoid accumulation of the radiation induced SEUs in the LBs firmware.

Both LBs and CB are based on the Xilinx Spartan III FPGAs, the CB additionally contains radiation-tolerant (FLASH based) FPGA Actel ProAsicPlus.

The High Voltage power system is located in USC, not exposed to radiation and easily accessible for any reparation. A single HV channel powers 2 RPC chambers both in the barrel and endcap regions. The Low Voltage boards are located in UXC on the balconies and provide the voltage to the front end electronics.

4.4.3   Pulse processing of CMS RPCs

Signals induced by cosmic particle in the RPC strips are shaped by standard CMS RPC Front-End Electronics (FEE) following the scheme of Figure 4.1. On a first stage, analogic signals are amplified and then sent to the Constant Fraction Discriminator (CFD) described in Figure 4.2. At the end of the chain, $100\,\text{ns}$ long pulses are sent in the LVDS output. These output signal are sent on one side to a V1190A Time-to-Digital Converter (TDC) module from CAEN and on the other to an OR module to count the number of detected signals. Trigger and hit coïncidences are monitored using scalers. The TDC is used to store the data into ROOT files. These files are thus analysed to understand the detectors performance.

(a)

(b)
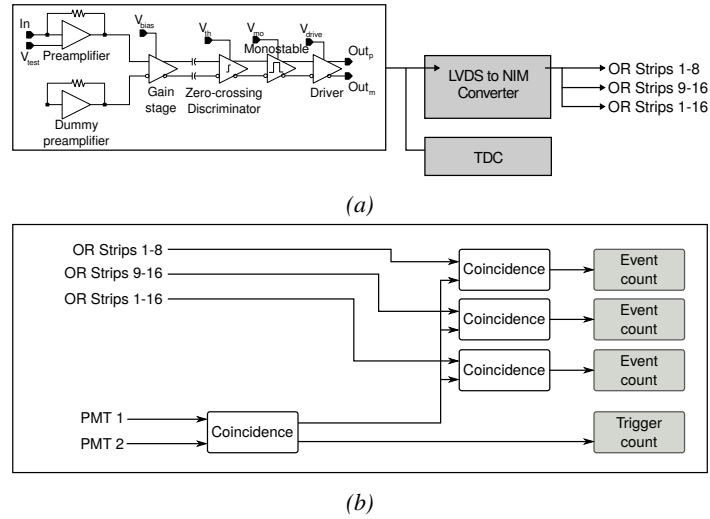
Figure 4.1: Signals from the RPC strips are shaped by the FEE described on Figure 4.1a. Output LVDS signals are then read-out by a TDC module connected to a computer or converted into NIM and sent to scalers. Figure 4.1b describes how these converted signals are put in coincidence with the trigger.

(a)

(b)
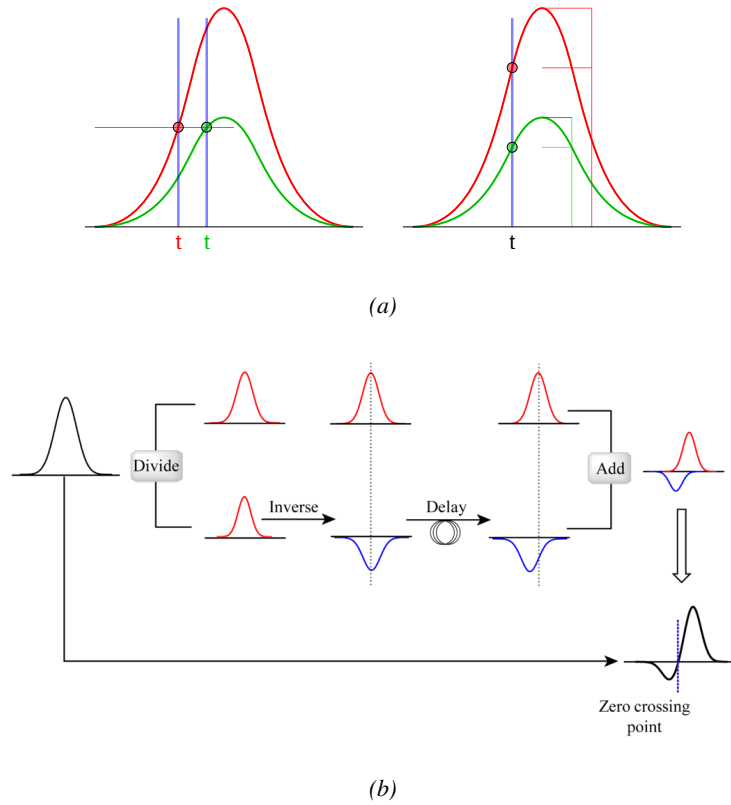
Figure 4.2: Description of the principle of a CFD. A comparison of threshold triggering (left) and constant franction triggering (right) is shown in Figure 4.2a. Constant franction triggering is obtained thanks to zero-crossing technique as explained in Figure 4.2b. The signal arriving at the input of the CFD is split into three components. A first one is delayed and connected to the inverting input of a first comparator. A second component is connected to the noninverting input of this first comparator. A third component is connected to the noninverting input of another comparator along with a threshold value connected to the inverting input. Finally, the output of both comparators is fed through an AND gate.

5

Longevity studies and Consolidation of the present CMS RPC subsystem

5.1 Testing detectors under extreme conditions

The upgrade from LHC to HL-LHC will increase the peak luminosity from 10^{34} $\text{cm}^{-2}\,\text{s}^{-1}$ to reach 5×10^{34} $\text{cm}^{-2}\,\text{s}^{-1}$, increasing in the same way the total expected background to which the RPC system will be subjected to. Composed of low energy gammas and neutrons from p-p collisions, low momentum primary and secondary muons, puch-through hadrons from calorimeters, and particles produced in the interaction of the beams with collimators, the background will mostly affect the regions of CMS that are the closest to the beam line, i.e. the RPC detectors located in the endcaps. [To update.]

The 2016 data allowed to study the values of the background rate in all RPC system. In Figure 5.1, the distribution of the chamber background hit rate per unit area is shown at a luminosity of $5 \times 10^{34} cm^{-2}.s^{-1}$ linearly extrapolating from data collected in 2016 [ref mentioning the linear dependency of rate vs lumi]. The maximum rate per unit area at HL-LHC conditions is expected to be of the order of $600 Hz/cm^2$ (including a safety factor 3). Nevertheless, Fluka simulations have conducted in order to understand the background at HL-LHC conditions. The comparison to the data has shown, in Figure 5.2, a discrepancy of a factor 2 even though the order of magnitude is consistent. [Understand mismatch.]
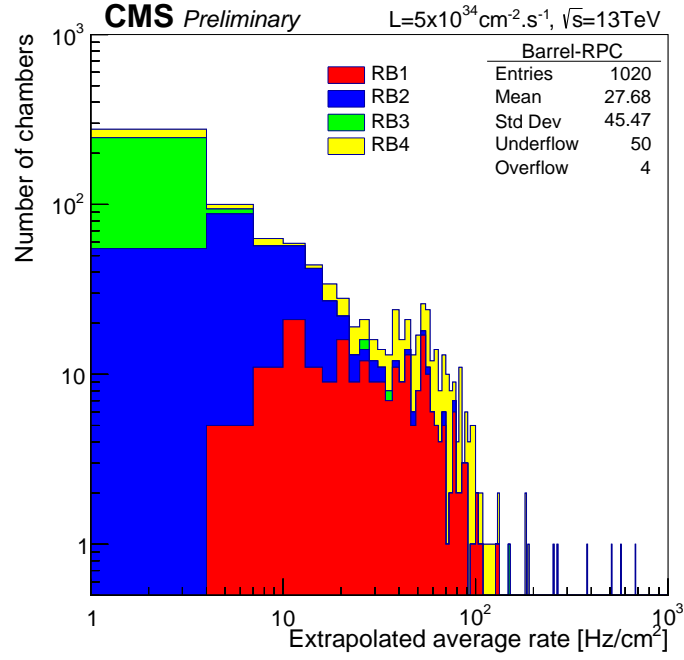
(a)
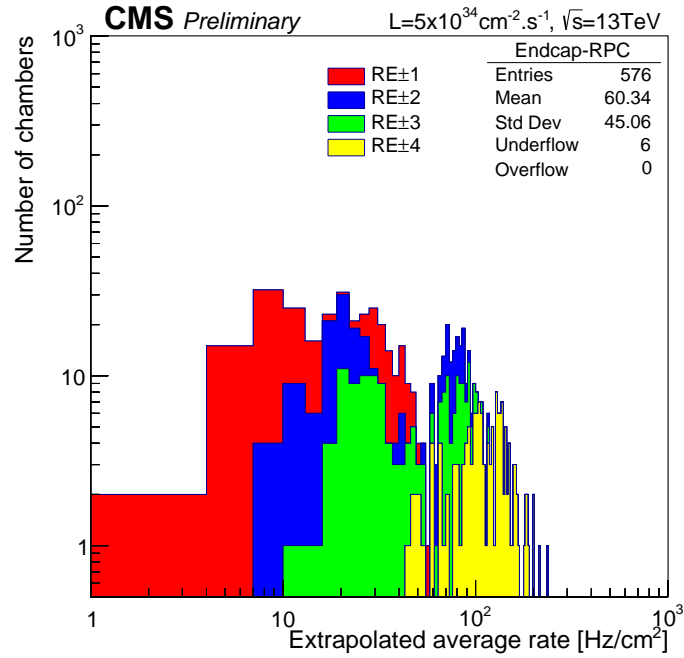
(b)

Figure 5.1: (5.1a) Extrapolation from 2016 data of single hit rate per unit area in the barrel region. (5.1b) Extrapolation from 2016 data of single hit rate per unit area in the endcap region.
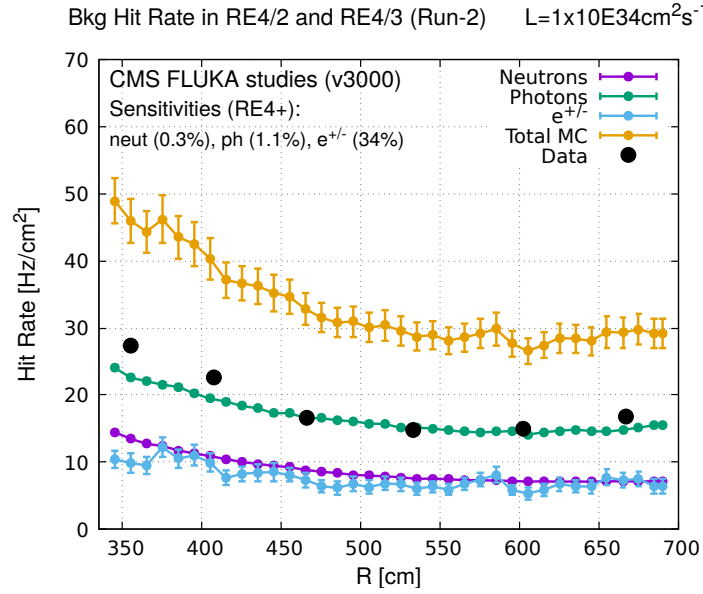
Figure 5.2: Background Fluka simulation compared to 2016 Data at $L = 10^{34}cm^{-2}.s^{-1}$ in the fourth endcap disk region. A mismatch in between simulation and data can be observed. [To be understood.]

In the past, extensive long-term tests were carried out at several gamma and neutron facilities certifying the detector performance. Both full size and small prototype RPCs have been irradiated with photons up to an integrated charge of $\sim 0.05C/cm^2$ and $\sim 0.4C/cm^2$, respectively [4, 5]. During Run-I, the RPC system provided stable operation and excellent performance and did not show any aging effects for integrated charge of the order of $0.01C/cm^2$. Projections on currents from 2016 Data, has allowed to determine that the total integrated charge, by the end of HL-LHC, would be of the order of $1C/cm^2$ (including a safety factor 3). [Corresponding figure needed.]

5.1.1 The Gamma Irradiation Facilities

5.1.1.1 GIF

Located in the SPS West Area at the downstream end of the X5 test beam, the Gamma Irradiation Facility (GIF) was a test area in which particle detectors were exposed to a particle beam in presence of an adjustable gamma background [6]. Its goal was to reproduce background conditions these detectors would suffer in their operating environment at LHC. GIF layout is shown in Figure 5.3. Gamma

photons are produced by a strong ^{137}Cs source installed in the upstream part of the zone inside a lead container. The source container includes a collimator, designed to irradiate a $6 \times 6\,\text{m}^2$ area at $5\,\text{m}$ maximum to the source. A thin lens-shaped lead filter helps providing with a uniform outcoming flux in a vertical plane, orthogonal to the beam direction. The principal collimator hole provides a pyramidal aperture of $74° \times 74°$ solid angle and provides a photon flux in a pyramidal volume along the beam axis. The photon rate is controled by further lead filters allowing the maximum rate to be limited and to vary within a range of four orders of magnitude. Particle detectors under test are then placed within the pyramidal volume in front of the source, perpendicularly to the beam line in order to profit from the homogeneous photon flux. Adjusting the background flux of photons can then be done by using the filters and choosing the position of the detectors with respect to the source.
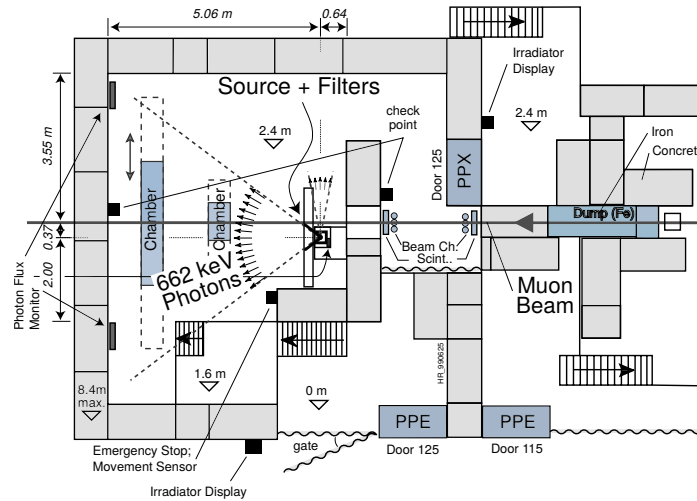
Figure 5.3: Layout of the test beam zone called X5c GIF at CERN. Photons from the radioactive source produce a sustained high rate of random hits over the whole area. The zone is surrounded by $8\,\text{m}$ high and $80\,\text{cm}$ thick concrete walls. Access is possible through three entry points. Two access doors for personnel and one large gate for material. A crane allows installation of heavy equipment in the area.

As described on Figure 5.4, the ^{137}Cs source emits a $662\,\text{keV}$ photon in 85% of the decays. An activity of $740\,\text{GBq}$ was measured on the 5th March 1997. To estimate the strength of the flux in 2014, it is necessary to consider the nuclear decay through time assiciated to the Cesium source whose half-life is well known ($t_{1/2} = (30.05 \pm 0.08)\,\text{y}$). The GIF tests where done in between the 20th and the 31st of August 2014, i.e. at a time $t = (17.47 \pm 0.02)\,\text{y}$ resulting in an attenuation

of the activity from $740\,\text{GBq}$ in 1997 to $494\,\text{GBq}$ in 2014.
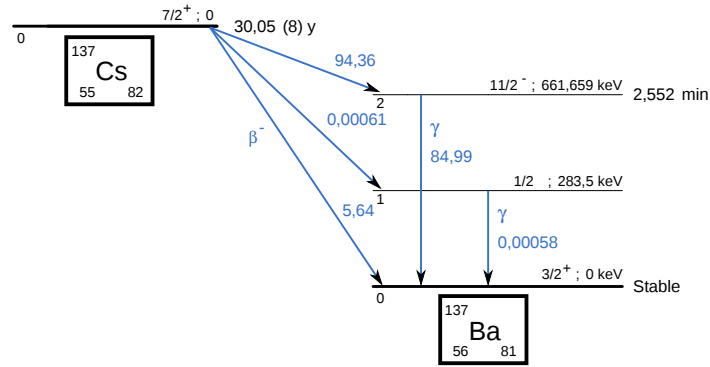
Figure 5.4: ^{137}Cs decays by β^- emission to the ground state of ^{137}Ba (BR = 5.64%) and via the $662\,\text{keV}$ isomeric level of ^{137}Ba (BR = 94.36%) whose half-life is 2.55 min.

5.1.1.2 GIF++

The new Gamma Irradiation Facility (GIF++), located in the SPS North Area at the downstream end of the H4 test beam, has replaced its predecessor during LS1 and has been operational since spring 2015 [7]. Like GIF, GIF++ features a ^{137}Cs source of $662\,\text{keV}$ gamma photons, their fluence being controlled with a set of filters of various attenuation factors. The source provides two separated large irradiation areas for testing several full-size muon detectors with continuous homogeneous irradiation, as presented in Figure 5.5.
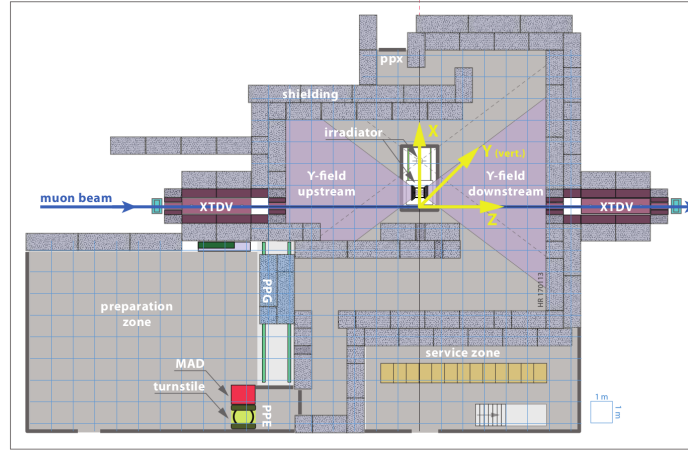
Figure 5.5: Floor plan of the GIF++ facility. When the facility downstream of the GIF++ takes electron beam, a beam pipe is installed along the beam line (z-axis). The irradiator can be displaced laterally (its center moves from $x = 0.65\,\mathrm{m}$ to $2.15\,\mathrm{m}$), to increase the distance to the beam pipe.

The source activity was measured to be about $13.5\,\mathrm{TBq}$ in March 2016. The photon flux being far greater than HL-LHC expectations, GIF++ provides an excellent facility for accelerated aging tests of muon detectors.

(a)

(b)
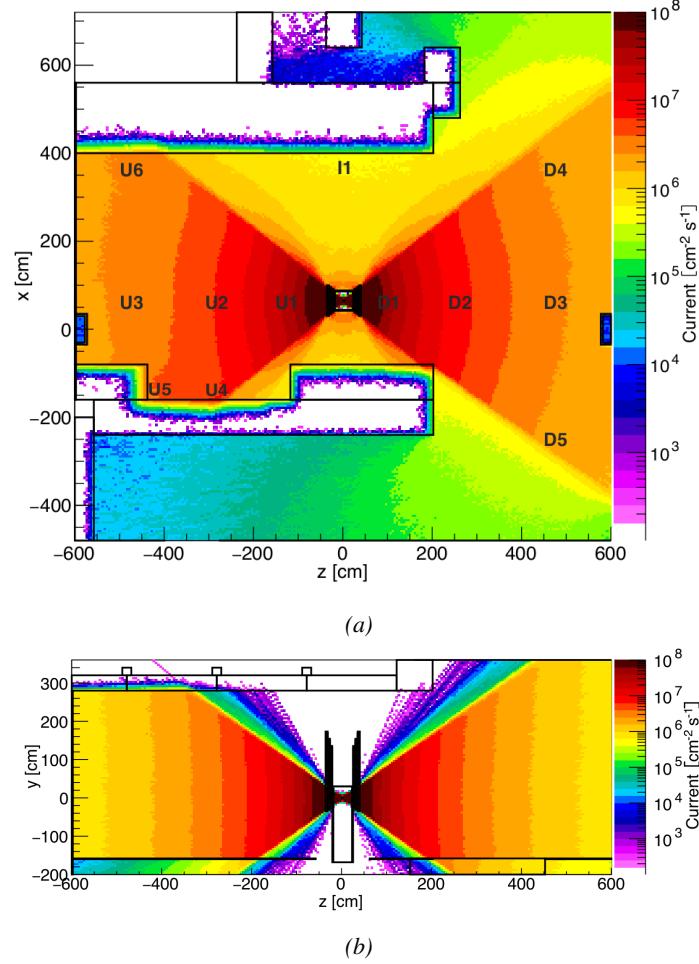
Figure 5.6: Simulated unattenuated current of photons in the xz plane (Figure 5.6a) and yz plane (Figure 5.6b) through the source at $x = 0.65$ m and $y = 0$ m. With angular correction filters, the current of 662 keV photons is made uniform in xy planes.

The source is situated in the muon beam line with the muon beam being available a few times a year. The H4 beam, composed of muons with a momentum of about 150 GeV/c, passes through the GIF++ zone and is used to study the performance of the detectors. Its flux is of 104 particles/s/cm^2 focused in an area similar to 10×10 cm^2. Therefore, with properly adjusted filters, one can imitate the HL-LHC background and study the performance of muon detectors with their trigger/readout electronics in HL-LHC environment.

5.2 Preliminary tests at GIF

5.2.1 Resistive Plate Chamber test setup

During summer 2014, preliminary tests have been conducted in the GIF area on a newly produced RE4/2 chamber labelled RE-4-2-BARC-161. This chamber has been placed into a trolley covered with a tent. The position of the RPC inside the tent and of the tent related to the source is described in Figure 5.7. To test this CMS RPC, three different absorber settings were used. First of all, measurements were done with fully opened source. Then, to complete this preliminary study, the gamma flux has been attenuated from a factor 2 and a factor 5. The expected gamma flux at the level of our detector will be discussed in subsection 5.2.4.
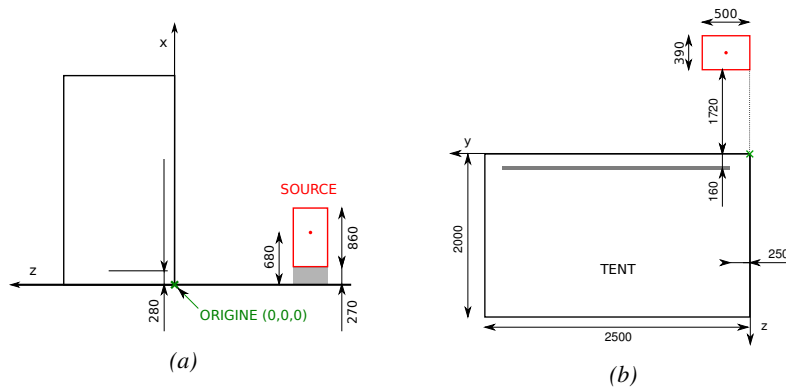
Figure 5.7: *Description of the RPC setup. Dimensions are given in* mm. *A tent containing RPCs is placed at* 1720 mm *from the source container. The source is situated in the center of the container. RE-4-2-BARC-161 chamber is* 160 mm *inside the tent. This way, the distance between the source and the chambers plan is* 2060 mm. *Figure 5.7a provides a side view of the setup in the* xz *plane while Figure 5.7b shows a top view in the* yz *plane.*
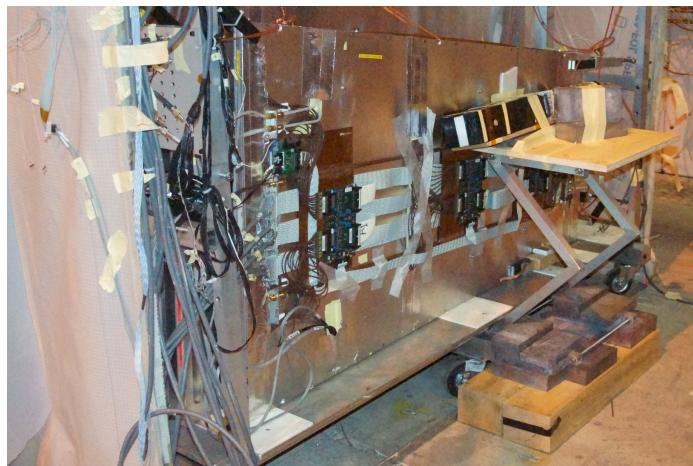
Figure 5.8: RE-4-2-BARC-161 chamber is inside the tent as described in Figure 5.7. In the top right, the two scintillators used as trigger can be seen. This trigger system has an inclination of $10°$ relative to horizontal and is placed above half-partition B2 of the RPCs. PMT electronics are shielded thanks to lead blocks placed in order to protect them without stopping photons from going through the scintillators and the chamber.

At the time of the tests, the beam not being operationnal anymore, a trigger composed of 2 plastic scintillators has been placed in front of the setup with an inclination of $10 \deg$ with respect to the detector plane in order to look at cosmic muons. Using this particular trigger layout, shown on Figure 5.8, leads to a cosmic muon hit distribution into the chamber similar to the one in Figure 5.9. Measured without gamma irradiation, two peaks can be seen on the profil of partition B, centered on strips 52 and 59. Section 5.2.3 will help us undertand that these two peaks are due respectively to forward and backward coming cosmic particles where forward coming particles are first detected by the scintillators and then the RPC while the backward coming muons are first detected in the RPC.
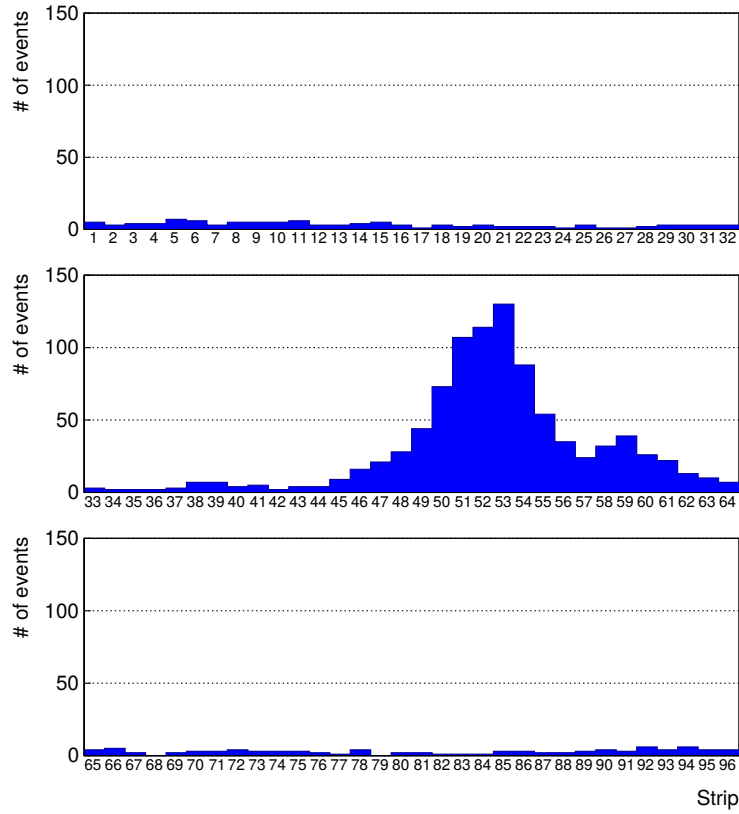
Figure 5.9: Hit distributions over all 3 parttions of RE-4-2-BARC-161 chamber is showed on these plots. Top, middle and bottom figures respectively correspond to partitions A, B, and C. These plots show that some events still occur in other half-partitions than B2, which corresponds to strips 49 to 64, in front of which the trigger is placed, contributing to the inefficiency of detection of cosmic muons. In the case of partitions A and C, the very low amount of data can be interpreted as noise. On the other hand, it is clear that a little portion of muons reach the half-partition B1, corresponding to strips 33 to 48.

5.2.2 Data Acquisition

5.2.3 Geometrical acceptance of the setup layout to cosmic muons

In order to profit from a constant gamma irradiation, the detectors inside of the GIF bunker need to be placed in a plane orthogonal to the beam line. The muon beam that used to be available was meant to test the performance of detectors under test. This beam not being active anymore, another solution to test detector performance had to be used. Thus, it has been decided to use cosmic muons detected through

a telescope composed of two scintillators. Lead blocks were used as shielding to protect the photomultipliers from gammas as can be seen from Figure 5.8.

An inclination has been given to the cosmic telescope to maximize the muon flux. A good compromise had to be found between good enough muon flux and narrow enough hit distribution to be sure to contain all the events into only one half partitions as required from the limited available readout hardware. Nevertheless, a consequence of the misplaced trigger, that can be seen as a loss of events in half-partition B1 in Figure 5.9, is an inefficiency. Nevertheless, the innefficiency of approximately 20 % highlighted in Figure 5.10 by comparing the performance of chamber BARC-161 in 904 and at GIF without irradiation seems too important to be explained only by the geometrical acceptance of the setup itself. Simulations have been conducted to show how the setup brings inefficiency.
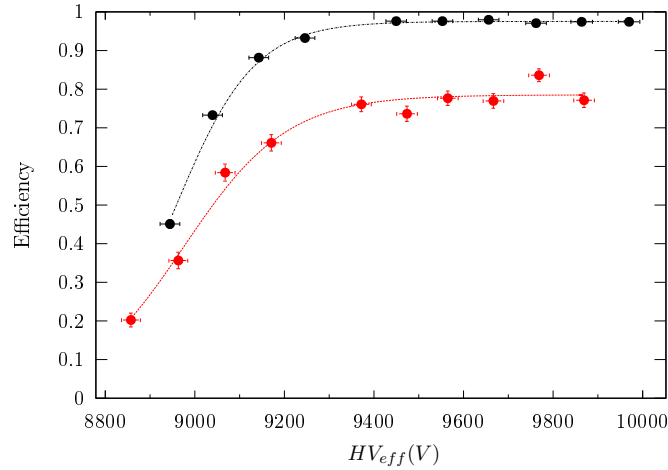
Figure 5.10: Results are derived from data taken on half-partition B2 only. On the 18th of June 2014, data has been taken on chamber RE-2-BARC-161 at building 904 (Prevessin Site) with cosmic muons providing us a reference efficiency plateau of $(97.54 \pm 0.15)\%$ represented by a black curve. A similar measurement has been done at GIF on the 21st of July with the same chamber giving a plateau of $(78.52 \pm 0.94)\%$ represented by a red curve.

5.2.3.1 Description of the simulation layout

The layout of GIF setup has been reproduced and incorporated into a Monte Carlo (MC) simulation to study the influence of the disposition of the telescope on the final distribution measured by the RPC. A 3D view of the simulated layout is given into Figure 5.11. Muons are generated randomly in a horizontal plane located at a height corresponding to the lowest point of the PMTs. This way, the needed size of the plane in order to simulate events happening at very big azimutal angles (i.e.

637 $\theta \approx \pi$) can be kept relatively small. The muon flux is designed to follow the usual
638 $cos^2\theta$ distribution for cosmic particle. The goal of the simulation is to look at
639 muons that pass through the muon telescope composed of the two scintilators and
640 define their distribution onto the RPC plane. During the reconstruction, the RPC
641 plane is then divided into its strips and each muon track is assigned to a strip.

(a)

(b)
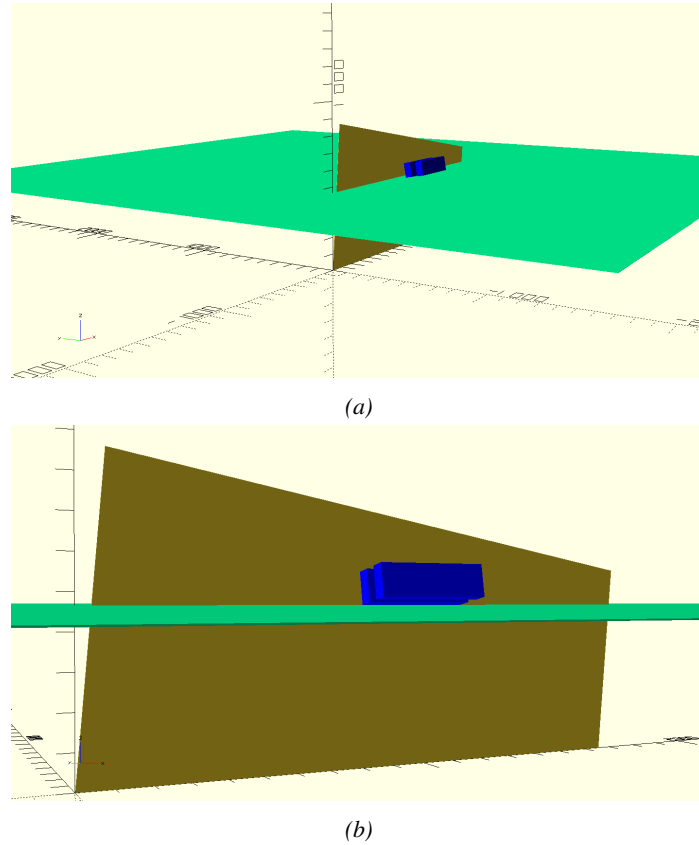
Figure 5.11: Representation of the layout used for the simulations of the test setup. The RPC is represented as a yellow trapezoid while the two scintillators as blue cuboids looking at the sky. A green plane corresponds to the muon generation plane within the simulation. Figure 5.7a shows a global view of the simulated setup. Figure 5.7b shows a zommed view that allows to see the 2 scintillators as well as the full RPC plane.

642 In order to further refine the quality of the simulation and understand deeper
643 the results the dependance of the distribution has been studied for a range of tele-
644 scope inclinations. Moreover, the threshold applied on the PMT signals has been
645 included into the simulation in the form of a cut. In the approximation of uni-
646 form scintillators, it has been considered that the threshold can be understood as

647 the minimum distance particles need to travel through the scintillating material to
648 give a strong enough signal. Particles that travel a distance smaller than the set
649 "threshold" are thus not detected by the telescope and cannot trigger the data tak-
650 ing. Finally, the FEE threshold also has been considered in a similar way. The
651 mean momentum of horizontal cosmic rays is higher than those of vertical ones
652 but the stopping power of matter for momenta ranging from $1\,\mathrm{GeV}$ to $1\,\mathrm{TeV}$ stays
653 comparable. It is then possible to assume that the mean number of primary e^-/ion
654 pairs per unit length will stay similar and thus, depending on the applied discrimi-
655 nator threshold, muons with the shortest path through the gas volume will deposit
656 less charge and induce a smaller signal on the pick-up strips that could eventu-
657 ally not be detected. These two thresholds also restrain the overall geometrical
658 acceptance of the system.

5.2.3.2 Simulation procedure

660 The simulation software has been designed using C++ and the output data is saved
661 into ROOT histograms. Simulations start for a threshold T_{scint} varying in a range
662 from 0 to $45\,\mathrm{mm}$ in steps of $5\,\mathrm{mm}$, where $T_{scint} = 0\,\mathrm{mm}$ corresponds to the case
663 where there isn't any threshold apply on the input signal while $T_{scint} = 45\,\mathrm{mm}$,
664 which is the scintillator thickness, is the case where muons cannot arrive orthogo-
665 nally onto the scintillator surface. For a given T_{scint}, a set of RPC thresholds are
666 considered. The RPC threshold, T_{RPC} varies from $2\,\mathrm{mm}$, the thickness of the gas
667 volume, to $3\,\mathrm{mm}$ in steps of $0.25\,\mathrm{mm}$. For each $(T_{scint};T_{RPC})$ pair, $N_\mu = 10^8$
668 muons are randomly generated inside the muon plane described in the previous
669 paragraph with an azimutal angle θ chosen to follow a $cos^2\theta$ distribution.

670 Planes are associated to each surface of the scintillators. Knowing muon posi-
671 tion into the muon plane and its direction allows us, by assuming that muons travel
672 in a straight line, to compute the intersection of the muon track with these planes.
673 Applying conditions to the limits of the surfaces of the scintillator faces then gives
674 us an answer to weither or not the muon passed through the scintillators. In the
675 case the muon has indeed passed through the telescope, the path through each scin-
676 tillator is computed and muons whose path was shorter than T_{scint} are rejected and
677 are thus considered as having not interacted with the setup.

678 On the contrary, if the muon is labeled as good, its position within the RPC
679 plane is computed and the corresponding strip, determined by geometrical tests
680 in the case the distance through the gas volume was enough not to be rejected
681 because of T_{RPC}, gets a hit and several histograms are filled in order to keep
682 track of the generation point on the muon plane, the intersection points of the
683 reconstructed muons within the telescope, or on the RPC plane, the path traveled
684 through each individual scintillator or the gas volume, as well as other histograms.
685 Moreover, muons fill different histograms weither they are forward or backward
686 coming muons. They are discriminated according to their direction components.

687 When a muon is generated, an (x, y, z) position is assigned into the muon plane as
688 well as a $(\theta; \phi)$ pair that gives us the direction it's coming from. This way, muons
689 satisfying the condition $0 \leq \phi < \pi$ are designated as backward coming muons
690 while muons satisfying $\pi \leq \phi < 2\pi$ as forward coming muons.

691 This simulation is then repeated for different telescope inclinations ranging in
692 between 4 and $20°$ and varying in steps of $2°$. Due to this inclination and to the
693 vertical position of the detector under test, the muon distribution reconstructed in
694 the detector plane is asymmetrical. The choice as been made to chose a skew
695 distribution formula to fit the data built as the multiplication of gaussian and sig-
696 moidal curves together. A typical gaussian formula is given as 5.1 and has three
697 free parameters as A_g, its amplitude, $\bar{x}$, its mean value and σ, its root mean square.
698 Sigmoidal curves as given by formula 5.2 are functions converging to 0 and A_s as
699 x diverges. The inflexion point is given as x_i and λ is proportional to the slope at
700 $x = x_i$. In the limit where $\lambda \longrightarrow \infty$, the sigmoid becomes a step function.

$$g(x) = A_g e^{\frac{-(x-\bar{x})^2}{2\sigma^2}} \tag{5.1}$$

$$s(x) = \frac{A_s}{1 + e^{-\lambda(x-x_i)}} \tag{5.2}$$

701 Finally, a possible representation of a skew distribution is given by formula 5.3
702 and is the product of 5.1 and 5.2. Naturally, here $A_{sk} = A_g \times A_s$ and represents
703 the theoretical maximum in the limit where the skew tends to a gaussian function.

$$sk(x) = g(x) \times s(x) = A_{sk} \frac{e^{\frac{-(x-\bar{x})^2}{2\sigma^2}}}{1 + e^{-\lambda(x-x_i)}} \tag{5.3}$$

704 ### 5.2.3.3   Results

705 **Influence of T_{scint} on the muon distribution**

706 **Influence of T_{RPC} on the muon distribution**

707 **Influence of the telescope inclination on the muon distribution**

708 **Comparison to data taken at GIF without irradiation**

5.2.4   Photon flux at GIF

5.2.4.1   Expectations from simulations

In order to understand and evaluate the γ flux in the GIF area, simulations had been conducted in 1999 and published by S. Agosteo et al [6]. Table 5.1 presented in this article gives us the γ flux for different distances D to the source. This simulation was done using GEANT and a Monte Carlo N-Particle (MCNP) transport code, and the flux F is given in number of γ per unit area and unit time along with the estimated error from these packages expressed in %.

Nominal	Photon flux F [s^{-1}cm^{-2}]			
ABS	at $D = 50$ cm	at $D = 155$ cm	at $D = 300$ cm	at $D = 400$ cm
1	$0.12 \cdot 10^8 \pm 0.2\%$	$0.14 \cdot 10^7 \pm 0.5\%$	$0.45 \cdot 10^6 \pm 0.5\%$	$0.28 \cdot 10^6 \pm 0.5\%$
2	$0.68 \cdot 10^7 \pm 0.3\%$	$0.80 \cdot 10^6 \pm 0.8\%$	$0.25 \cdot 10^6 \pm 0.8\%$	$0.16 \cdot 10^6 \pm 0.6\%$
5	$0.31 \cdot 10^7 \pm 0.4\%$	$0.36 \cdot 10^6 \pm 1.2\%$	$0.11 \cdot 10^6 \pm 1.2\%$	$0.70 \cdot 10^5 \pm 0.9\%$

Table 5.1: Total photon flux ($E\gamma \leq 662$ keV) with statistical error predicted considering a ^{137}Cs activity of 740 GBq at different values of the distance D to the source along the x-axis of irradiation field [6].
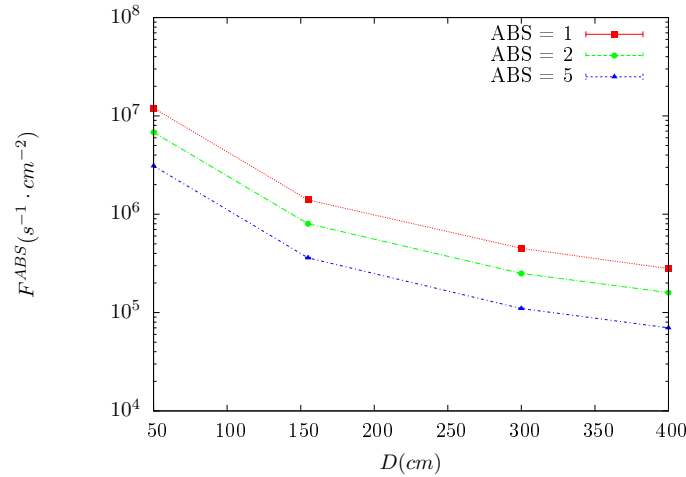
Figure 5.12: γ flux $F(D)$ is plot using values from table 5.1. As expected, the plot shows similar attenuation behaviours with increasing distance for each absorption factors.

The simulation doesn't directly provides us with an estimated flux at the level of our RPC. First of all, it is needed to extract the value of the flux from the available data contained in the original paper and then to estimate the flux in 2014 at the time the experimentation took place. Figure 5.12 that contains the data from

Table 5.1. In the case of a pointlike source emiting isotrope and homogeneous gamma radiations, the gamma flux F at a distance D to the source with respect to a reference point situated at D_0 where a known flux F_0 is measured will be expressed like in Equation 5.4, assuming that the flux decreases as $1/D^2$, where c is a fitting factor.

$$F^{ABS} = F_0^{ABS} \times \left(\frac{cD_0}{D} \right)^2 \tag{5.4}$$

By rewriting Equation 5.4, it comes that :

$$c = \frac{D}{D_0} \sqrt{\frac{F^{ABS}}{F_0^{ABS}}} \tag{5.5}$$

$$\Delta c = \frac{c}{2} \left(\frac{\Delta F^{ABS}}{F^{ABS}} + \frac{\Delta F_0^{ABS}}{F_0^{ABS}} \right) \tag{5.6}$$

Finally, using Equation 5.5 and the data in Table 5.1 with $D_0 = 50\,\text{cm}$ as reference point, we can build Table 5.2. It is interesting to note that c for each value of D doesn't depend on the absorption factor.

| Nominal | Correction factor c | | |
ABS	at $D = 155\,\text{cm}$	at $D = 300\,\text{cm}$	at $D = 400\,\text{cm}$
1	$1.059 \pm 0.70\%$	$1.162 \pm 0.70\%$	$1.222 \pm 0.70\%$
2	$1.063 \pm 1.10\%$	$1.150 \pm 1.10\%$	$1.227 \pm 0.90\%$
5	$1.056 \pm 1.60\%$	$1.130 \pm 1.60\%$	$1.202 \pm 1.30\%$

Table 5.2: Correction factor c is computed thanks to formulae 5.5 taking as reference $D_0 = 50\,\text{cm}$ and the associated flux F_0^{ABS} for each absorption factor available in table 5.1.

For the range of D/D_0 values available, it is possible to use a simple linear fit to get the evolution of c. The linear fit will then use only 2 free parameters, a and b, as written in Equation 5.7. This gives us the results showed in Figure 5.13. Figure 5.13b confirms that using only a linear fit to extract c is enough as the evolution of the rate that can be obtained superimposes well on the simulation points.

$$c \left(\frac{D}{D_0} \right) = a \frac{D}{D_0} + b \tag{5.7}$$

$$F^{ABS} = F_0^{ABS} \left(a + \frac{bD_0}{D} \right)^2 \tag{5.8}$$

$$\Delta F^{ABS} = F^{ABS} \left[\frac{\Delta F_0^{ABS}}{F_0^{ABS}} + 2 \frac{\Delta a + \Delta b \frac{D_0}{D}}{a + \frac{bD_0}{D}} \right] \tag{5.9}$$

(a)

(b)
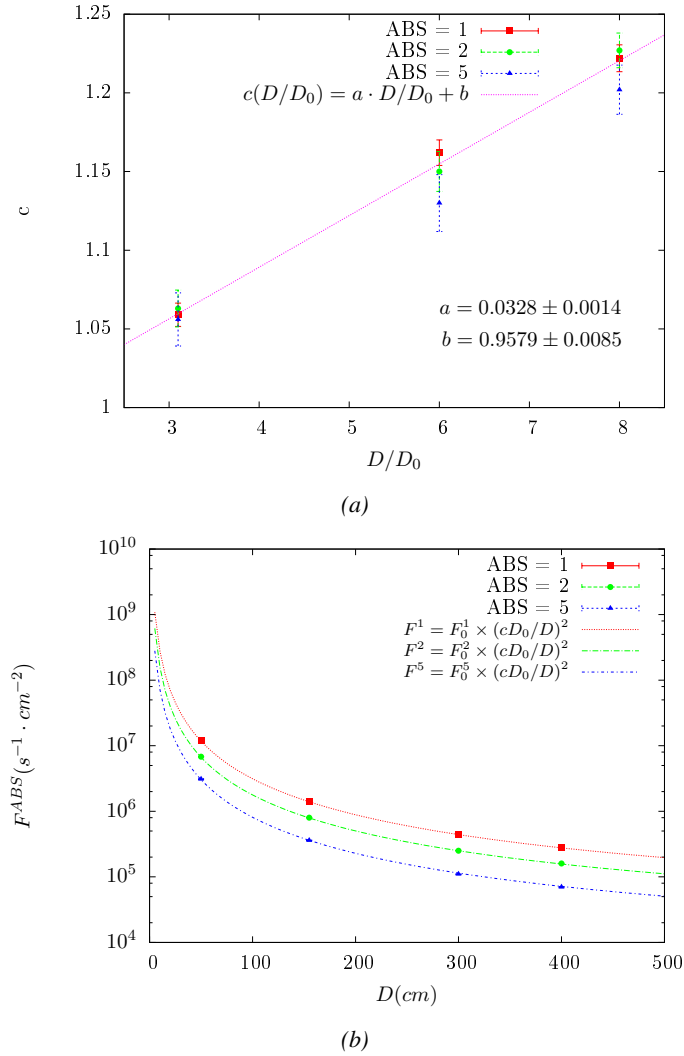
Figure 5.13: Figure 5.13a shows the linear approximation fit done via formulae 5.7 on data from table 5.2. Figure 5.13b shows a comparison of this model with the simulated flux using a and b given in figure 5.13a in formulae 5.4 and the reference value $D_0 = 50cm$ and the associated flux for each absorption factor F_0^{ABS} from table 5.1

In the case of the 2014 GIF tests, the RPC plane is located at a distance $D = 206$ cm to the source. Moreover, to estimate the strength of the flux in 2014, it is necessary to consider the nuclear decay through time assiciated to the Cesium source whose half-life is well known ($t_{1/2} = (30.05 \pm 0.08)$ y). The very first source activity measurement has been done on the 5th of March 1997 while the

GIF tests where done in between the 20th and the 31st of August 2014, i.e. at a time $t = (17.47 \pm 0.02)$ y resulting in an attenuation of the activity from $740\,\text{GBq}$ in 1997 to $494\,\text{GBq}$ in 2014. All the needed information to extrapolate the flux through our detector in 2014 has now been assembled, leading to the Table 5.3. It isinteresting to note that for a common RPC sensitivity to γ of $2 \cdot 10^{-3}$, the order of magnitude of the estimated hit rate per unit area is of the order of the kHz for the fully opened source. Moreover, taking profit of the two working absorbers, it will be possible to scan background rates at $0\,\text{Hz}$, $\sim 300\,\text{Hz}$ as well as $\sim 600\,\text{Hz}$. Without source, a good estimate of the intrinsic performance will be available. Then at $300\,\text{Hz}$, the goal will be to show that the detectors fulfill the performance certification of CMS RPCs. Then a first idea of the performance of the detectors at higher background will be provided with absorbtion factors 2 ($\sim 600\,\text{Hz}$) and 1 (no absorbtion). *[Here I will also put a reference to the plot showing the estimated background rate at the level of RE3/1 in the case of HL-LHC but this one being in another chapter, I will do it later.]*

| Nominal | Photon flux F [$\text{s}^{-1}\text{cm}^{-2}$] | | | Hit rate/unit area [$\text{Hz}\,\text{cm}^{-2}$] |
ABS	at $D_0^{1997} = 50\,\text{cm}$	at $D^{1997} = 206\,\text{cm}$	at $D^{2014} = 206\,\text{cm}$	at $D^{2014} = 206\,\text{cm}$
1	$0.12 \cdot 10^8 \pm 0.2\%$	$0.84 \cdot 10^6 \pm 0.3\%$	$0.56 \cdot 10^6 \pm 0.3\%$	1129 ± 32
2	$0.68 \cdot 10^7 \pm 0.3\%$	$0.48 \cdot 10^6 \pm 0.3\%$	$0.32 \cdot 10^6 \pm 0.3\%$	640 ± 19
5	$0.31 \cdot 10^7 \pm 0.4\%$	$0.22 \cdot 10^6 \pm 0.3\%$	$0.15 \cdot 10^6 \pm 0.3\%$	292 ± 9

Table 5.3: The data at D_0 in 1997 is taken from [6]. In a second step, using Equations 5.8 and 5.9, the flux at D can be estimated in 1997. Then, taking into account the attenuation of the source activity, the flux at D can be estimated at the time of the tests in GIF in 2014. Finally, assuming a sensitivity of the RPC to γ $s = 2 \cdot 10^{-3}$, an estimation of the hit rate per unit area is obtained.

5.2.4.2 Dose measurements
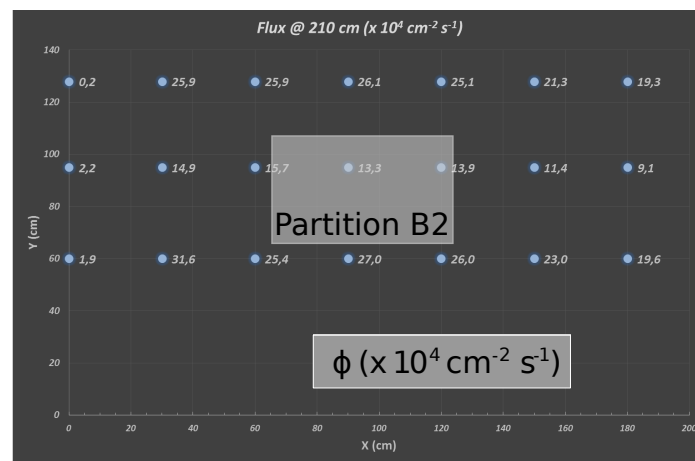
Figure 5.14: Dose measurements has been done in a plane corresponding to the tents front side. This plan is 1900 mm away from the source. As explained in the first chapter, a lens-shaped lead filter provides a uniform photon flux in the vertical plan orthogonal to the beam direction. If the second line of measured fluxes is not taken into account because of lower values due to experimental equipments in the way between the source and the tent, the uniformity of the flux is well showed by the results.

757 **5.2.5 Results and discussions**

(a)   *(b)*

(c)   *(d)*
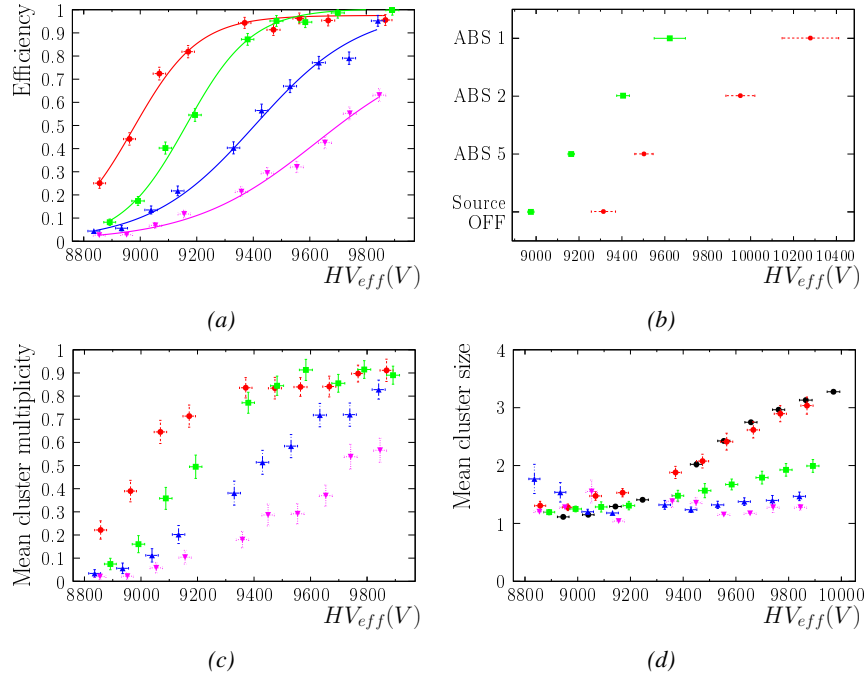
Figure 5.15

5.3   Longevity tests at GIF++

Longevity studies imply a monitoring of the performance of the detectors probed using a high intensity muon beam in a irradiated environment by periodically measuring their rate capability, the dark current running through them and the bulk resistivity of the Bakelite composing their electrodes. GIF++, with its very intense ^{137}Cs source, provides the perfect environment to perform such kind of tests. Assuming a maximum acceleration factor of 3, it is expected to accumulate the equivalent charge in 1.7 years.

As the maximum background is found in the endcap, the choice naturally was made to focus the GIF++ longevity studies on endcap chambers. Most of the RPC system was installed in 2007. Nevertheless, the large chambers in the fourth endcap (RE4/2 and RE4/3) have been installed during LS1 in 2014. The Bakelite of these two different productions having different properties, four spare chambers of the present system were selected, two RE2,3/2 spares and two RE4/2 spares. Having two chambers of each type allows to always keep one of them non irradiated as reference, the performance evolution of the irradiated chamber being then compared through time to the performance of the non irradiated one.

The performance of the detectors under different level of irradiation is measured periodically during dedicated test beam periods using the H4 muon beam. In between these test beam periods, the two RE2,3/2 and RE4/2 chambers selected for this study are irradiated by the ^{137}Cs source in order to accumulate charge and the gamma background is monitored, as well as the currents. The two remaining chambers are kept non-irradiated as reference detectors. Due to the limited gas flow in GIF++, the RE4 chamber remained non-irradiated until end of November 2016 where a new mass flow controller has been installed allowing for bigger volumes of gas to flow in the system.

Figures 5.16 and 5.17 give us for different test beam periods, and thus for increasing integrated charge through time, a comparison of the maximum efficiency, obtained using a sigmoid-like function, and of the working point of both irradiated and non irradiated chambers [8]. No aging is yet to see from this data, the shifts in γ rate per unit area in between irradiated and non irradiated detectors and RE2 and RE4 types being easily explained by a difference of sensitivity due to the various Bakelite resistivities of the HPL electrodes used for the electrode production.

Collecting performance data at each test beam period allows us to extrapolate the maximum efficiency for a background hit rate of $300\,\mathrm{Hz/cm}^2$ corresponding to the expected HL-LHC conditions. Aging effects could emerge from a loss of efficiency with increasing integrated charge over time, thus Figure 5.18 helps us understand such degradation of the performance of irradiated detectors in comparison with non irradiated ones. The final answer for an eventual loss of efficiency is given in Figure 5.19 by comparing for both irradiated and non irradiated detectors

798   the efficiency sigmoids before and after the longevity study. Moreover, to complete
799   the performance information, the Bakelite resistivity is regularly measured thanks
800   to Ag scans (Figure 5.20) and the noise rate is monitored weekly during irradiation
801   periods (Figure 5.21). At the end of 2016, no signs of aging were observed and
802   further investigation is needed to get closer to the final integrated charge require-
803   ments proposed for the longevity study of the present CMS RPC sub-system.
804

(a)   *(b)*
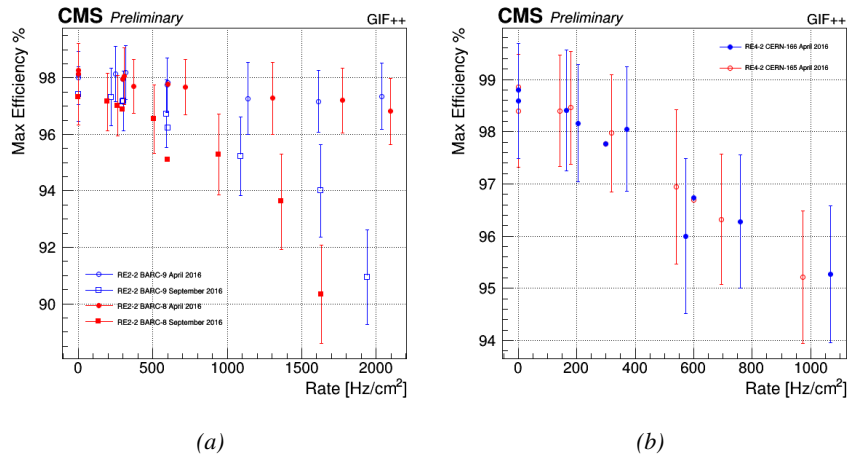
*Figure 5.16: Evolution of the maximum efficiency for RE2 (5.16a) and RE4 (5.16b) cham-
bers with increasing extrapolated γ rate per unit area at working point. Both irradiated
(blue) and non irradiated (red) chambers are shown.*
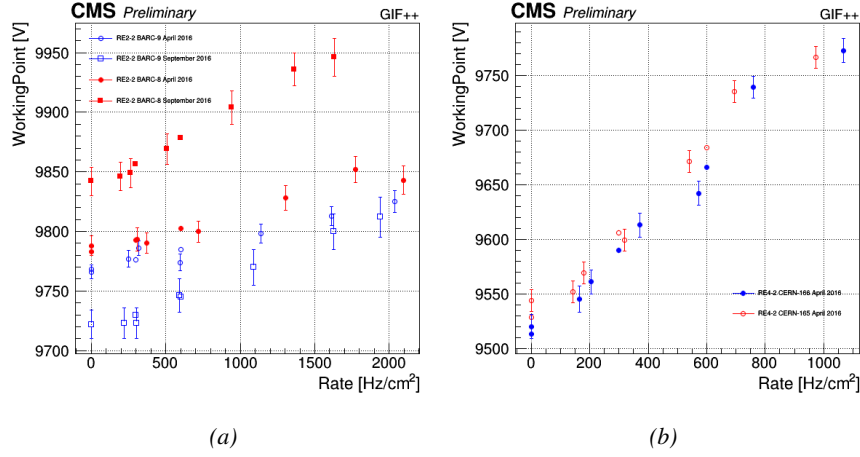
Figure 5.17: Evolution of the working point for RE2 (5.17a) and RE4 (5.17b) with increasing extrapolated γ rate per unit area at working point. Both irradiated (blue) and non irradiated (red) chambers are shown.
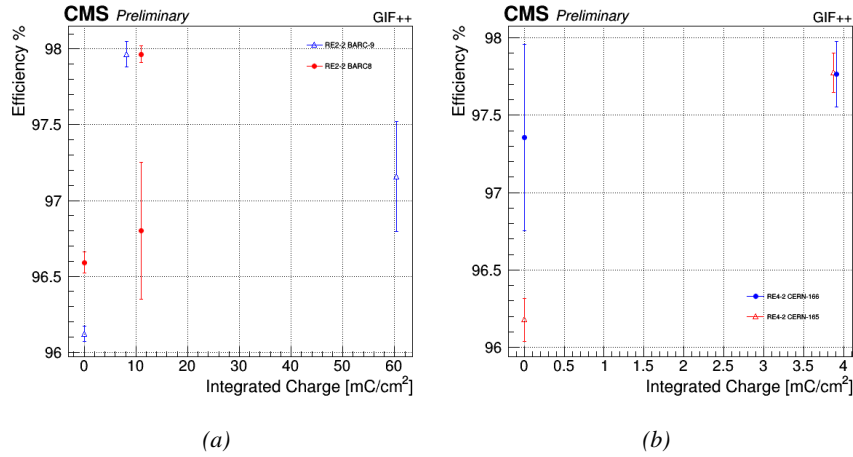
Figure 5.18: Evolution of the maximum efficiency at HL-LHC conditions, i.e. a background hit rate per unit area of $300\,\mathrm{Hz/cm^2}$, with increasing integrated charge for RE2 (5.18a) and RE4 (5.18b) detectors. Both irradiated (blue) and non irradiated (red) chambers are shown. The integrated charge for non irradiated detectors is recorded during test beam periods and stays small with respect to the charge accumulated in irradiated chambers.
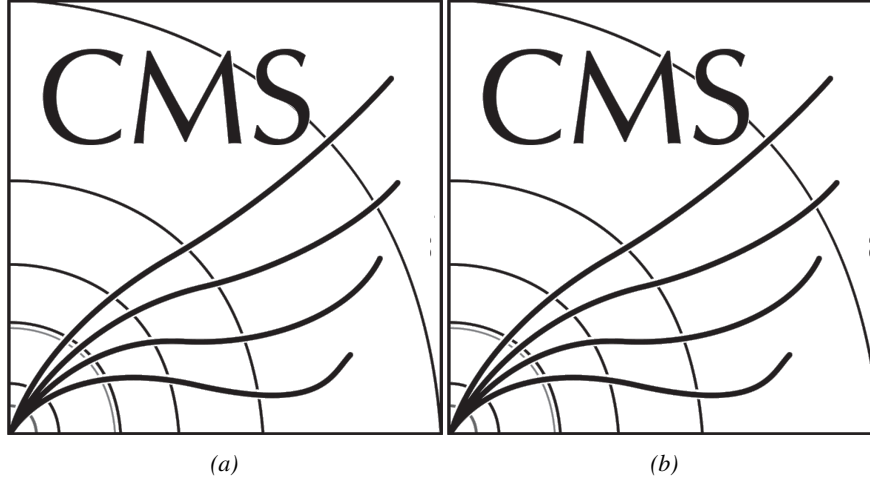
Figure 5.19: Comparison of the efficiency sigmoid before (triangles) and after (circles) irradiation for RE2 (5.19a) and RE4 (5.19b) detectors. Both irradiated (blue) and non irradiated (red) chambers are shown.
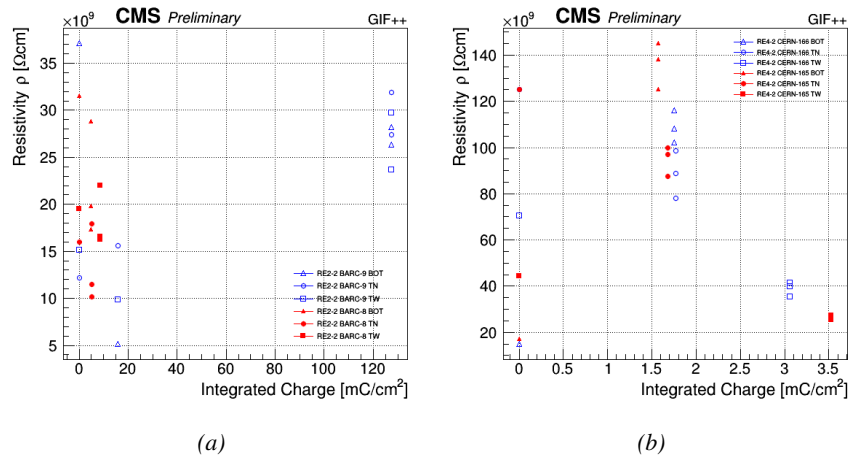
Figure 5.20: Evolution of the Bakelite resistivity for RE2 (5.20a) and RE4 (5.20b) detectors. Both irradiated (blue) and non irradiated (red) chambers are shown.
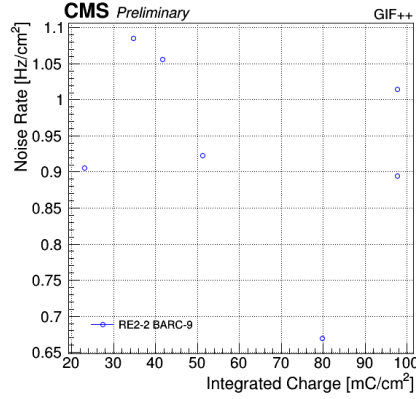
Figure 5.21: Evolution of the noise rate per unit area for the irradiated chamber RE2-2-BARC-9 only.

5.3.1 Description of the Data Acquisition

For the longevity studies, four spare chambers of the present system are used. Two spare RPCs of the RE2,3 stations as well as two spare RPCs from the new RE4 stations have been mounted in a Trolley. Six RE4 gaps are also placed in the trolley. The trolley is placed inside the GIF++ in the upstream region of the bunker, taking the cesium source as a reference. The trolley is oriented for the detection surface of the chambers to be orthogonal to the beam line. The system can be moved along the orthogonal plane in order to have the beam in all η-partitions. For the aging the trolley is moved outside the beam line and is placed in a distance of $5.2\,\mathrm{m}$ to the source, which irradiates the bunker using an attenuation filter of 2.2 which corresponds to a fluence of $10^7 \mathrm{gamma/cm}^2$.

During GIF++ operation, the data collected can be divided into different categories as several parameters are monitored in addition to the usual RPC performance data. On one hand, to know the performance of a chamber, it is need to measure its efficiency and to know the background conditions in which it is operated. To do this, the hit signals from the chamber are recorded and stored in a ROOT file via a Data Acquisition (DAQ) software. On the other hand, it is also very important to monitor parameters such as environmental pressure and temperature, gas temperature and humidity, RPC HV, LV, and currents, or even source and beam status. This is done through the GIF++ web Detector Control Software (DCS) that stores this information in a database.

Two different types of tests are conducted on RPCs via the DAQ. Indeed, the performance of the detectors is measured periodically during dedicated test beam periods using the H4 muon beam. In between these test beam periods, when the beam is not available, the chambers are irradiated by the ^{137}Cs in order to accu-

mulate deposited charge and the gamma background is measured.

RPCs under test are connected through LVDS cables to V1190A Time-to-Digital Converter (TDC) modules manufactured by CAEN. These modules, located in the rack area outside of the bunker, get the logic signals sent by the chambers and save them into their buffers. Due to the limited size of the buffers, the collected data is regularly erased and replaced. A trigger signal is needed for the TDC modules to send the useful data to the DAQ computer via a V1718 CAEN USB communication module.

In the case of performance test, the trigger signal used for data acquisition is generated by the coincidence of three scintillators. A first one is placed upstream outside of the bunker, a second one is placed downstream outside of the bunker, while a third one is placed in front of the trolley, close by the chambers. Every time a trigger is sent to the TDCs, i.e. every time a muon is detected, knowing the time delay in between the trigger and the RPC signals, signals located in the right time window are extracted from the buffers and saved for later analysis. Signals are taken in a time window of $400\,\mathrm{ns}$ centered on the muon peak (here we could show a time spectrum). On the other hand, in the case of background rate measurement, the trigger signal needs to be "random" not to measure muons but to look at gamma background. A trigger pulse is continuously generated at a rate of $300\,\mathrm{Hz}$ using a dual timer. To integrate an as great as possible time, all signals contained within a time window of 10us prior to the random trigger signal are extracted form the buffers and saved for further analysis (here another time spectrum to illustrate could be useful, maybe even place both spectrum together as a single Figure).

The signals sent to the TDCs correspond to hit collections in the RPCs. When a particle hits a RPC, it induce a signal in the pickup strips of the RPC readout. If this signal is higher than the detection threshold, a LVDS signal is sent to the TDCs. The data is then organised into 4 branches keeping track of the event number, the hit multiplicity for the whole setup, and the time and channel profile of the hits in the TDCs.

5.3.2   RPC current, environmental and operation parameter monitoring

In order to take into account the variation of pressure and temperature between different data taking periods the applied voltage is corrected following the relationship :

$$HVeff = HVapp \times \left(0.2 + 0.8 \cdot \frac{P_0}{P} \times \frac{T}{T_0} \right) \qquad (5.10)$$

where T_0 (=293 K) and P_0 (=990 mbar) are the reference values.

5.3.3 Measurement procedure

Insert a short description of the online tools (DAQ, DCS, DQM).

Insert a short description of the offline tools : tracking and efficiency algorithm.

Identify long term aging effects we are monitoring the rates per strip.

5.3.4 Longevity studies results

6

Investigation on high rate RPCs

6.1 Rate limitations and ageing of RPCs

6.1.1 Low resistivity electrodes

6.1.2 Low noise front-end electronics

6.2 Construction of prototypes

6.3 Results and discussions

7

Conclusions and outlooks

7.1 Conclusions

7.2 Outlooks

References

[1] CERN. Geneva. LHC Experiments Committee. *The CMS muon project : Technical Design Report*. Tech. rep. CERN-LHCC-97-032. CMS Collaboration, 1997.

[2] CERN. Geneva. LHC Experiments Committee. *Technical Proposal for the Phase-II Upgrade of the CMS Detector*. Tech. rep. CERN-LHCC-2015-010. CMS Collaboration, 2015.

[3] CERN. Geneva. LHC Experiments Committee. *CMS, the Compact Muon Solenoid : technical proposal*. Tech. rep. CERN-LHCC-94-38. CMS Collaboration, 1994.

[4] M. Abbrescia et al. "Study of long-term performance of CMS RPC under irradiation at the CERN GIF". In: *NIMA* 533 (2004), pp. 102–106.

[5] H.C. Kim et al. "Quantitative aging study with intense irradiation tests for the CMS forward RPCs". In: *NIMA* 602 (2009), pp. 771–774.

[6] S. Agosteo et al. "A facility for the test of large-area muon chambers at high rates". In: *NIMA* 452 (2000), pp. 94–104.

[7] PoS, ed. *CERN GIF ++ : A new irradiation facility to test large-area particle detectors for the high-luminosity LHC program*. Vol. TIPP2014. 2014, pp. 102–109.

[8] M. Abbrescia et al. "Cosmic ray tests of double-gap resistive plate chambers for the CMS experiment". In: *NIMA* 550 (2005), pp. 116–126.

[9] A. Fagot. *GIF++ DAQ v4.0*. 2017. URL: https://github.com/afagot/GIF_DAQ.

[10] CAEN. *Mod. V1190-VX1190 A/B, 128/64 Ch Multihit TDC*. 14th ed. 2016.

[11] CAEN. *Mod. V1718 VME USB Bridge*. 9th ed. 2009.

[12] W-Ie-Ne-R. *VME 6021-23 VXI*. 5th ed. 2016.

A

A data acquisition software for CAEN VME TDCs

Certifying detectors in the perspective of HL-LHC required to develop tools for the GIF++ experiment. Among them was the Data Acquisition (DAQ) software that allows to make the communications in between the computer and the TDC modules in order to retrieve the RPC data [9]. In this appendix, details about the software, as of how the software was written, how it functions and how it can be exported to another similar setup.

A.1   Description of the setup

The CMS RPC setup at GIF++ counts 5 V1190A Time-to-Digital Converter (TDC) manufactured by CAEN [10]. The communication between the computer and the TDCs to transfer data is done via a V1718 VME master module also manufactured by CAEN and operated from a USB port [11]. These VME modules are hosted into a 6U VME 6021 powered crate manufactured by W-Ie-Ne-R than can accomodate up to 21 VME bus cards [12]. These 3 components of the DAQ setup are shown in Figure A.1.
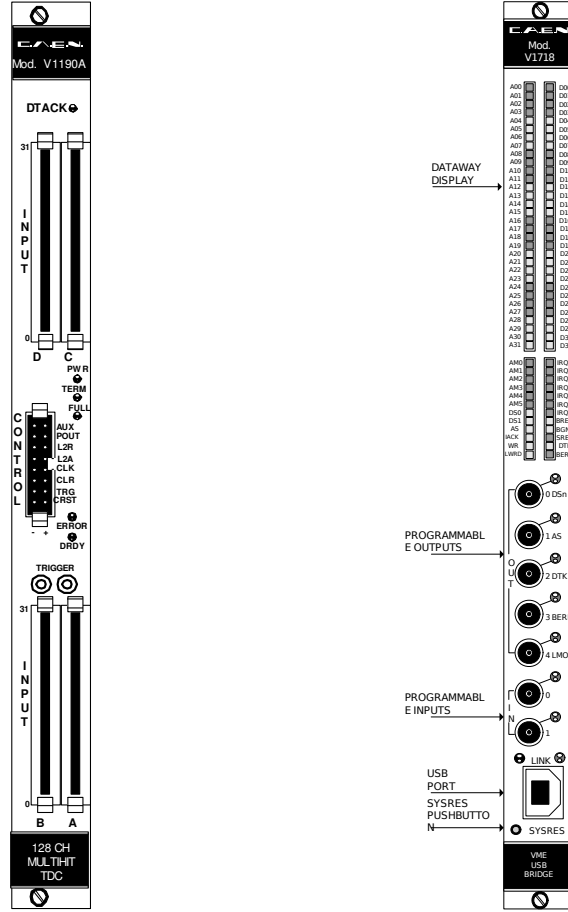
(a)   *(b)*

(c)

Figure A.1: (A.1a) View of the front panel of a V1190A TDC module [10]. (A.1b) View of the front panel of a V1718 Bridge module [11]. (A.1c) View of the front panel of a 6U 6021 VME crate [12].

A.2 Data read-out

To efficiently perform a data readout algorithm, objects to handle the VME modules (TDCs and VME bridge) have been created along with objects to store data and read the configuration file that comes as an input of the DAQ software.
It is useful to remind that the DAQ software in GIF++ is not a standalone software but is called through a Web Detector Control System (webDCS) application, that is the core of interactions with GIF++ setup, when data needs to be taken. Nevertheless, it is straight forward to make it into a standalone program that could be adapted to any VME setup using V1190A and V1718 modules.

A.2.1 V1190A TDCs

The DAQ used at GIF takes profit of the *Trigger Matching Mode* offered by V1190A modules. A trigger matching is performed in between a trigger time tag and the channel time measurements. Control over this data acquisition mode, explained through Figure A.2, is offered through 4 programmable parameters:

- **match window:** the match between a trigger and a hit is done within a programmable time window. This is set via the method
  `v1190a::SetTrigWindowWidth(Uint windowWidth,`**`int`**` ntdcs)`

- **window offset:** temporal distance between the trigger tag and the start of the trigger matching window. This is set via the method
  `v1190a::SetTrigWindowWidth(Uint windowWidth,`**`int`**` ntdcs)`

- **extra search margin:** an extended time window is used to ensure that all matching hits are found. This is set via the method
  `v1190a::SetTrigSearchMargin(Uint searchMargin,`**`int`**` ntdcs)`

- **reject margin:** older hits are automatically rejected to preven buffer overflows and to speed up the search time. This is set via the method
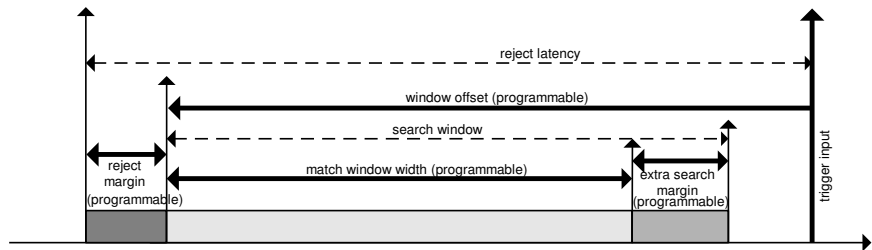 `v1190a::SetTrigRejectionMargin(Uint rejectMargin,`**`int`**` ntdcs)`

Figure A.2: Module V1190A Trigger Matching Mode timing diagram [10].

Each of these 4 parameters are given in number of clocks, 1 clock being 25 ns long. It is easy to understand at this level that there are 3 possible functionning settings:

- **1:** the match window is entirely contained after the trigger signal,

- **2:** the match window overlaps the trigger signal, or

- **3:** the match window is entirely contained before the trigger signal as displayed on Figure A.2.

In both the first and second cases, the sum of the window width and of the offset can be set to a maximum of 40 clocks, which corresponds to 1 µs. Evidently, the offset can be negative, allowing for a longer match window, its further limit being at most 1 µs after the trigger signal. In the third case, the maximum negative offset allowed is of 2048 clocks (12 bit) corresponding to 51.2 µs, the match window being strictly smaller than the offset. In the case of GIF++, the choice has been made to use this last setting by delaying the trigger signal. During the studies performed in GIF++, both the efficiency of the RPCs, using a muon beam, and the noise or gamma background rate are monitored. The extra search and reject margins are left unused.

To probe the efficiency of RPC detectors, a signal provided by the coïncidence of scintillators when a bunch of muons passes through GIF++ area is used to trigger the data acquisition. For this measurement, it is useful to reduce the match window width only to contain the muon information. Indeed, the delay in between a trigger signal and the detection of the corresponding muon in the RPC being very contant (typically a few tens of ns due to jitter and cable length), the muon signals are very localised in time. Thus, due to a delay of approximalety 325 ns in between the muons and the trigger, the settings where chosen to have a window width of 24 clocks (600 ns) centered on the muon peak thanks to a negative offset of 29 clocks (725 ns).

On the otherhand, monitoring the rates doesn't require for the DAQ to look at a specific time window. It is important to integrate as much time as possible to have a robust measurement of the rate as the number of hits per time unit. The triggerring signal is provided by a pulse generator at a frequency of 300 Hz to ensure that the data taking occurs in a random way, with respect to beam physics, to probe only the irradiation spectrum on the detectors. The match window is set to 400 clocks (10 µs) and the negative offset to 401 clocks as it needs to exceed the value of the match window.

The v1190a object, defined in the DAQ software as followed, offer the possility to concatenate all TDCs in the setup into a single object containing a list of hardware addresses (addresses to access the TDC buffer through the VME crate)

and each constructor and method acts on the list of TDCs.

```cpp
class v1190a
{
 private :
    long               Handle;
    vector<Data32>    Address;
    CVDataWidth       DataWidth;
    CVAddressModifier AddressModifier;

 public:

    v1190a(long handle, IniFile *inifile, int ntdcs);
    ˜v1190a();
    Data16 write_op_reg(Data32 address, int code, string error);
    Data16 read_op_reg(Data32 address, string error);
    void    Reset(int ntdcs);
    void    Clear(int ntdcs);
    void    TestWR(Data16 value,int ntdcs);
    void    CheckTDCStatus(int ntdcs);
    void    CheckCommunication(int ntdcs);
    void    SetTDCTestMode(Data16 mode,int ntdcs);
    void    SetTrigMatching(int ntdcs);
    void    SetTrigTimeSubstraction(Data16 mode,int ntdcs);
    void    SetTrigWindowWidth(Uint windowWidth,int ntdcs);
    void    SetTrigWindowOffset(Uint windowOffset,int ntdcs);
    void    SetTrigSearchMargin(Uint searchMargin,int ntdcs);
    void    SetTrigRejectionMargin(Uint rejectMargin,int ntdcs);
    void    GetTrigConfiguration(int ntdcs);
    void    SetTrigConfiguration(IniFile *inifile,int ntdcs);
    void    SetTDCDetectionMode(Data16 mode,int ntdcs);
    void    SetTDCResolution(Data16 lsb,int ntdcs);
    void    SetTDCDeadTime(Data16 time,int ntdcs);
    void    SetTDCHeadTrailer(Data16 mode,int ntdcs);
    void    SetTDCEventSize(Data16 size,int ntdcs);
    void    SwitchChannels(IniFile *inifile,int ntdcs);
    void    SetIRQ(Data32 level, Data32 count,int ntdcs);
    void    SetBlockTransferMode(Data16 mode,int ntdcs);
    void    Set(IniFile *inifile,int ntdcs);
    void    CheckStatus(CVErrorCodes status) const;
    int     ReadBlockD32(Uint tdc, const Data16 address,
                Data32 *data, const Uint words, bool ignore_berr);
    Uint    Read(RAWData *DataList,int ntdcs);
};
```

A.2.2   V1718 USB Bridge

As previously described in Section 4.4.3, CMS RPC FEEs provide us with $100\,\mathrm{ns}$ long LVDS output signals that are injected into the TDCs' input. V1190A are VME units accepting 128 independent Multi-Hit/Multi-Event TDC channels whose signals are treated by 4 $100\,\mathrm{ps}$ high performance TDC chips developed by CERN / ECP-MIC Division. Any avalanche signal that gives a signal above the FEEs threshold is thus recorded by the TDCs as a hit within the match window. Each hit

is assigned to a specific TDC channel with a time stamp with a precision of 100 ps. The reference time, the 0, is provided by the beginning of the match window. thus for each trigger, coming from a scintillator coïncidence or the pulse generator, a list of hits is stored into the TDCs buffers and will then be transfered into a ROOT Tree.

The v1718 object is defined in the DAQ software as followed.

```cpp
class v1718{

    private :
        int                 Handle;

        Data32              Data;           // Data
        CVIRQLevels         Level;          // Interrupt level
        CVAddressModifier   AM;             // Addressing Mode
        CVDataWidth         DataSize;       // Data Format
        Data32              BaseAddress;    // Base Address

    public:
        v1718(IniFile *inifile);
        ~v1718();
        long                GetHandle(void) const;
        int                 SetData(Data16 data);
        Data16              GetData(void);
        int                 SetLevel(CVIRQLevels level);
        CVIRQLevels         GetLevel(void);
        int                 SetAM(CVAddressModifier am);
        CVAddressModifier   GetAM(void);
        int                 SetDatasize(CVDataWidth datasize);
        CVDataWidth         GetDataSize(void);
        int                 SetBaseAddress(Data16 baseaddress);
        Data16              GetBaseAddress(void);
        void                CheckStatus(CVErrorCodes status) const;
        bool                CheckIRQ();
        void                SetPulsers();
        void                SendBUSY(BusyLevel level);
};
```

A.2.3 DataReader

```cpp
class DataReader
{
    private:
        bool     StopFlag;
        IniFile *iniFile;
        Data32   MaxTriggers;
        v1718   *VME;
        int      nTDCs;
        v1190a  *TDCs;
        RAWData  TDCData;

    public:
        DataReader();
        virtual ~DataReader();
        void     SetIniFile(string inifilename);
        void     SetMaxTriggers();
        Data32   GetMaxTriggers();
        void     SetVME();
        void     SetTDC();
        int      GetQFlag(Uint it);
        void     Init(string inifilename);
        void     FlushBuffer();
        void     Update();
        string   GetFileName();
        void     WriteRunRegistry(string filename);
        void     Run();
};
```

The data transfer is done via Block Transfer (BLT). Using BLT allows to tranfer a fixed number of events called a *block*. This is used together with an Almost Full Level (AFL) of the TDCs' output buffers. This AFL gives the maximum amount of 32 bits words that can writen in the buffer before an Interrupt Request (IRQ) is generated and seen by the VME Bridge, stopping the data acquisition to transfer the content of each TDC buffers before resuming. The AFL can, at maximum, be of 32735 words (16 bits). This number corresponds to the depth of the output buffer of a TDC. For each trigger, 6 words or more are written into the TDC buffer:

- **a global header** providing information of the event number since the beginning of the data acquisition,

- **a TDC header**,

- **the TDC data** (if any), 1 for each hit recorded during the event, providing the channel and the time stamp associated to the hit,

- **a TDC error** providing error flags,

- **a TDC trailer**,

- **a global trigger time tag** that provides the absolute trigger time relatively to the last reset, and

- **a global trailer** providing the total word count in the event.

When the BLT is used, it is easy to understand that the maximum number of words that have been set as ALF will not be a finite number of events or, at least, the number of events that would be recorded into the TDC buffers will not be a multiple of the block size. In the last BLT cycle to tranfer data, the number of events to transfer will most propably be lower than the block size. In that case, the TDC can add fillers at the end of the block but this option requires to send more data to the computer and is thus a little slower. Another solution is to finish the transfer after the last event by sending a bus error that states that the BLT reached the last event in the pile. This method has been chosen in GIF++.

Due to irradiation, an event in GIF++ can count up to 300 words per TDC. A limit of 4096 words (12 bits) has been set to generate IRQ which represent from 14 to almost 700 events depending on the average of hits collected per event. Then the block size has been set to 100 events with enabled bus errors. When an AFL is reached for one of the TDCs, the VME bridge stops the acquisition at the hardware level by sending a NIM pulse out of one of the 5 programmable outputs to the VETO of the coíndidence module where the trigger signals originate from. As long as this signal is ON, no trigger reaches the TDCs anymore.

The data is then transfered one TDC at a time into a structure called RAWData described below.

```
struct RAWData{
    vector<int>            *EventList;
    vector<int>            *NHitsList;
    vector<int>            *QFlagList;
    vector<vector<int> >   *ChannelList;
    vector<vector<float> > *TimeStampList;
};
```

Each event is saved into `TBranch` of a ROOT `TTree` as 3 integers that represent the event ID (`EventCount`), the number of hits read from the TDCs (`nHits`), the quality flag that provides information for any problem in the data transfer (`qflag`), and 2 lists of nHits elements containing the fired TDC channel (`TDCCh`) and their respective time stamps (`TDCTS`).

```
RAWData TDCData;
TFile *outputFile = new TFile(outputFileName.c_str(),"recreate");
TTree *RAWDataTree = new TTree("RAWData","RAWData");

int          EventCount = -9;
int          nHits = -8;
int          qflag = -7;
vector<int>  TDCCh;
vector<float> TDCTS;

RAWDataTree->Branch("EventNumber",&EventCount, "EventNumber/I");
RAWDataTree->Branch("number_of_hits",&nHits,"number_of_hits/I");
RAWDataTree->Branch("Quality_flag",&qflag,"Quality_flag/I");
RAWDataTree->Branch("TDC_channel",&TDCCh);
RAWDataTree->Branch("TDC_TimeStamp",&TDCTS);

//...
//Here read the TDC data and place it into TDCData for as long
//as you didn't collect the requested amount of data.
//...

for(Uint i=0; i<TDCData.EventList->size(); i++){
    EventCount  = TDCData.EventList->at(i);
    nHits       = TDCData.NHitsList->at(i);
    qflag       = TDCData.QFlagList->at(i);
    TDCCh       = TDCData.ChannelList->at(i);
    TDCTS       = TDCData.TimeStampList->at(i);
    RAWDataTree->Fill();
}
```

A.2.4   DAQ algorithm overview

A.3   Software export

B

Details on the online analysis package

B.1 Introduction

insert text here

C

Structure of the hybrid simulation software

C.1 Introduction

insert text here...